

# Crystal growth and in-plane optical properties of Tl-Ba-Ca-Cu-O superconductors

Y. C. Ma and N.L. Wang\*

*Beijing National Laboratory for Condensed Matter Physics, Institute of Physics,  
Chinese Academy of Sciences, Beijing 100080, People's Republic of China*

(Dated: May 23, 2019)

Single crystals of thallium-based cuprates with the general formula  $Tl_2Ba_2Ca_{n-1}Cu_nO_x$  ( $n=1,2,3$ ) have been grown by the flux method. The superconducting transition temperatures determined by the ac magnetic susceptibility are 92 K, 109 K, and 119 K for  $n=1,2,3$  respectively. X-ray diffraction measurements and EDX compositional analysis were described. We measured in-plane optical reflectance from room temperature down to 10 K, placing emphasis on Tl-2223. The reflectance roughly has a linear-frequency dependence above superconducting transition temperature, but displays a pronounced knee structure together with a dip-like feature at higher frequency below  $T_c$ . Correspondingly, the ratio of the reflectances below and above  $T_c$  displays a maximum and a minimum near those feature frequencies. In particular, those features in Tl2223 appear at higher energy scale than Tl2212, and Tl2201. The optical data are analyzed in terms of spectral function. We discussed the physical consequences of the data in terms of both clean and dirty limit.

PACS numbers: 74.25.Gz, 74.72.Jt

## I. INTRODUCTION

Since the discovery of the high temperature superconductors (HTSC) in the 1980's, many experiments have been done to disclose the microscopic origin of high temperature superconductivity. For example, inelastic neutron scattering revealed a peculiar magnetic resonance mode at an energy of 41 meV in two-dimensional reciprocal lattice position  $(\pi, \pi)$  for optimally doped  $YBa_2Cu_3O_{6+\delta}$  [1, 2]. The angle resolved photoemission spectroscopy (ARPES) has indicated a kink in the band dispersion as well as an anisotropic gap (the d-wave behavior) for some high- $T_c$  cuprates [1, 3, 4]. These results are very helpful for understanding the superconductivity mechanism in the cuprates. Naturally, one may ask whether these behaviors are generic in HTSC materials. But there are technical reasons why those experimental probes have not been used with success on all the families of HTSCs. For example, inelastic neutron scattering experiment requires large-size single crystals and had mostly been done on YBCO-123 and LSCO-214 [1, 2, 5], although some groups have tried to work on  $Tl_2Ba_2CuO_{6+\delta}$  by synthesizing about 300 relatively large (0.5 to 3 mm<sup>3</sup>) single crystals and co-aligning them in a mosaic of total volume 0.11 cm<sup>3</sup> [6], as well as on  $Bi_2Sr_2CaCu_2O_{8+\delta}$  with a comparatively large single crystal of volume 10 × 5 × 1.2 mm<sup>3</sup> and mosaicity (that is, the angular spread of the crystallographic axes),  $\sim 1^\circ$  [7]. Tunnelling spectroscopy and ARPES are surface-sensitive probes. They are mainly applied to Bi-based cuprate systems as they could be cleaved easily in a vacuum along the Bi-O planes, yielding a high-quality virgin surface [1]. However, technique like optical spectroscopy places relatively less demands on the sample size

and surface, and have consequently been applied with success to a larger number of high temperature superconducting systems. At present, optical probes cover a wide frequency and temperature range, which have provided much useful information about charge excitations and dynamics of cuprate superconductors.

In the whole HTSC families, thallium-based cuprates have provided a large series of superconductors including single Tl-O layered compounds with the number of CuO<sub>2</sub> layers from 1 to 5 and double Tl-O layered compounds  $Tl_2Ba_2Ca_{n-1}Cu_nO_x$  with the CuO<sub>2</sub> layers  $n$  from 1 to 3 (hereafter abbreviated as Tl-2201, Tl-2212, Tl-2223, respectively) [8, 9, 10, 11, 12, 13, 14, 15]. The Tl-based cuprates offer a good opportunity to investigate the physical properties of systems with different number of CuO<sub>2</sub> layers in a unit cell, and therefore different  $T_c$  at the optimal doping. This will help to understand the mechanism of high temperature superconductivity. Another advantage of Tl-based cuprates is that, all the double Tl-O layer based cuprates have higher  $T_c$ s than the double Bi-O layer based cuprates with the same structure. Even for the single CuO<sub>2</sub> layered compound Tl-2201, its  $T_c$  can reach 90 K. Consequently, the difference between the superconducting state and the normal state can be easily probed. Nevertheless, despite those advantages, much less spectroscopic studies have been done on the Tl-based cuprates. This is mainly due to the difficulty of obtaining high quality single crystal samples. One has to overcome the problem of avoiding the poisonous thallium volatility and formation of intergrowth defects during crystal growth [12]. Infrared studies have been done on crystals of single-layered Tl-2201 [16, 17], and thin-films of double-layered Tl-2212 [18], but there is still no report, to the best of our knowledge, on triple-layered Tl-2223 and any other Tl-based superconductors.

We have recently successfully grown single crystals of  $Tl_2Ba_2Ca_{n-1}Cu_nO_x$  compounds with  $n=1,2$ , and 3 by the flux method. In this study, we first describe the

\*Email: nlwang@aphy.iphy.ac.cn

TABLE I: Nominal compositions in starting materials for crystal growth and transition temperatures of grown crystals Tl-Ba-Ca-Cu-O[11]:

Sample No.	Starting material Tl/Ba/Ca/Cu	$T_c$ K	Size mm <sup>2</sup>	Phase
A	2/2/0/1	92	1.2×1.5	Tl-2201
B	2/2/2/3	109	2.0×1.8	Tl-2212
C	2/2/6/6	119	1.2×0.9	Tl-2223

crystal growth procedure and characterization of the as grown crystals by the ac magnetic susceptibility, X-ray diffraction measurements and EDX compositional analysis. Then, we report the measurement of the in-plane infrared reflectance. As optical data for optimally doped Tl-2201 and Tl-2212 are available in literature, we place emphasis on the spectra collected on triple-layered Tl-2223 crystals and their comparisons with data of Tl-2212 and Tl-2201. Very similar to the Tl-2201 and Tl-2212, we observe significant change of spectra after entering superconducting state, which was related to the combination of a Boson mode and a gap. We analyzed the spectra in terms of spectral function. A linear scaling is established between the energy of the characteristic feature and the superconducting transition temperature for different systems at optimal doping.

## II. CRYSTAL GROWTH AND CHARACTERISTICS

Single crystals were grown by the flux method from raw materials with nominal compositions as listed in Table I. The mixed oxide BaCaCuO powders were synthesized prior to the crystal growth. For example, we made the BaCaCuO-223x powder for Tl-2212, and BaCaCuO-266x for Tl-2223. Then, Tl<sub>2</sub>O<sub>3</sub> powder was added into the mixed powders to get a stoichiometry as in Table I. The ratio of the oxide powders is essential for the crystal phase growth.

In the growth experiment, the powders of amount  $\sim$ 15 grams were ground in an agate mortar, then placed in an alumina crucible and covered with two Al<sub>2</sub>O<sub>3</sub> lids for decreasing the volatility of Tl<sub>2</sub>O<sub>3</sub>. The crucible was put in a tube furnace with flowing oxygen, and heated up to a high temperature for several hours. The temperature was set to be different for growing Tl-2201, Tl-2212, and Tl-2223 systems as shown in Fig. 1. The furnace was cooled down slowly at a rate of about 10°C per hour to certain temperature (depending on the system), then down to room temperature naturally. The oxygen flowed all the time during the sintering process. The starting temperature and the cooling rate seriously affect the size of a as-grown crystal. It also affects substantially the superconducting transition temperature of Tl-2201 phase.

From the experiments we find that the loss weight of Tl<sub>2</sub>O<sub>3</sub> is related to the sintering temperature and the time. Typically, Tl loss due to evaporation from a sealed

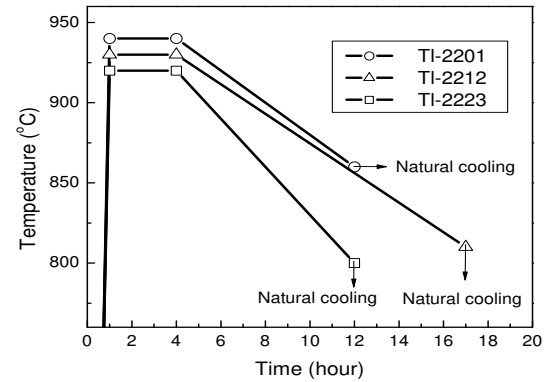


FIG. 1: The growth process for Tl-2201(a), Tl-2212(b) and Tl-2223 (c) single crystals.

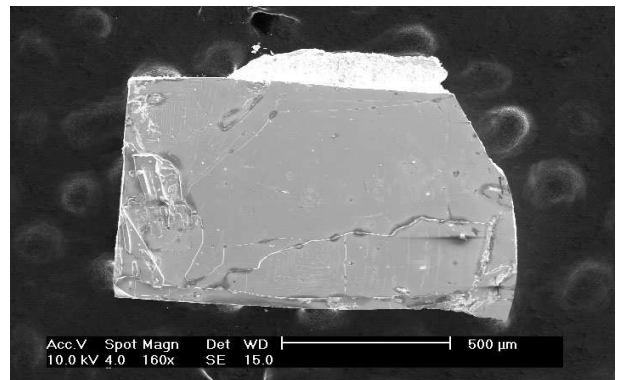


FIG. 2: SEM images of as grown crystals Tl-2223.

crucible is 7 to 20 percent of the total weight Tl<sub>2</sub>O<sub>3</sub>, so we add some more Tl<sub>2</sub>O<sub>3</sub> powders than the nominal ratio to compensate.

As the crucible had been cooled down to room temperature, the mm-sized crystals of Tl-2201, Tl-2212, and Tl-2223 single crystals has formed. Some shiny, usually free-standing crystals are found at the place near the cavities formed in the melt. The SEM images of a typical Tl-2223 crystal is shown in Fig.2.

According to X-ray diffraction measurements shown in Fig.3, nearly all the (0,0,l) peaks can be seen clearly, furthermore, no other phase can be seen in the diffraction pattern, and every sample has a good c-axial orientation which is perpendicular to the sample natural growth face. The half widths of midpoint of the X-ray diffraction peaks are typically 0.07°, 0.09° and 0.08° for Tl-2201, Tl-2212, and Tl-2223 single crystals, respectively. Clearly the intergrowth defects of the different members has been depressed by the sintering process. The lattice constants, c, of the three type of crystals are 23.21 Å, 29.28 Å and 35.55 Å for Tl-2201, Tl-2212, Tl-2223 phases, respectively, as there is a CuCaO<sub>2</sub> difference in each unit cell for the three phases.

The superconducting transition temperature  $T_c$  was determined by ac susceptibility measurement.  $T_c$  in-

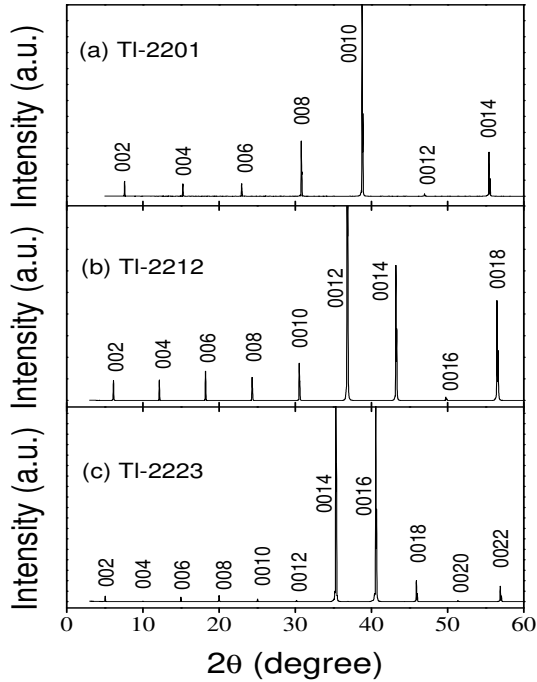


FIG. 3: The X-ray diffraction patterns up to 60 degree for (a)Tl-2201,(b)Tl-2212 and (c)Tl-2223.

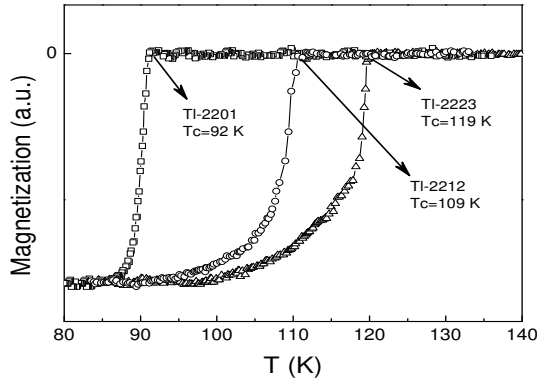


FIG. 4: Temperature dependence of ac susceptibility for Tl-2201, Tl-2212 and Tl-2223 single crystals. The maximum magnetization in each sample has been normalized.

creases in the three phases as the  $\text{CuO}_2$  layers in a unit cell increase from 1 to 3. The  $T_c$  for as-grown Tl-2212 and Tl-2223 crystals are always close to 109 K and 119 K, respectively, while the  $T_c$  for as-grown Tl-2201 crystals ranges from about 70 K to 92 K. Fig. 4 shows the temperature dependence of the ac susceptibility for as-grown Tl-2201, Tl-2212, and Tl-2223 single crystals.

The compositions of the crystals were examined by energy dispersive X-ray micro analysis(EDX). The quantitative measurements were performed at several points on the surface of the crystal, which show a good uniformity of composition on the crystal surface. Typical EDX spectra obtained from each phase of the crystal are shown in Fig.5. As expected form the ideal chemical

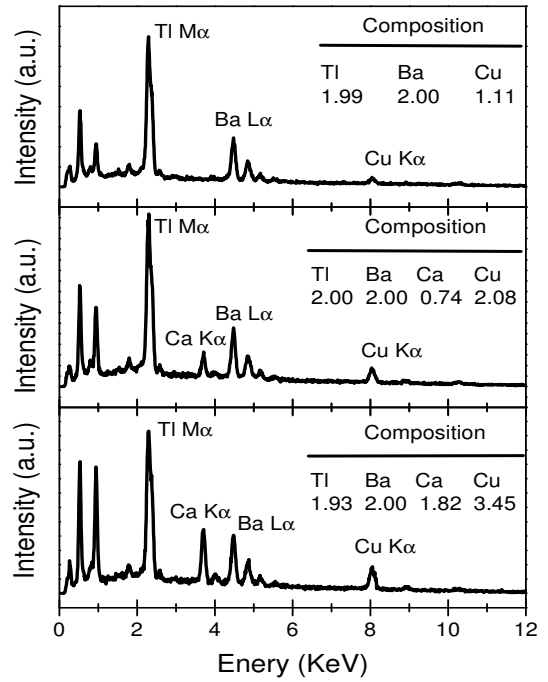


FIG. 5: EDX spectra and analyzed compositions for Tl-2201(a),Tl-2212(b) and Tl-2223 (c) phase. The compositions are calculated on the assumption that the molar ratio of Ba is the ideal value of two.

formula of each phase, the peak ratios of  $\text{CaK}\alpha/\text{BaL}\alpha$  and  $\text{CuK}\alpha/\text{BaL}\alpha$  in the EDX spectra increased with the number of Cu-O layers in Tl compounds. Note that there is no Ca in the Tl-2201 phase, this is because we did not mix the  $\text{CaO}$  before this phase has been formed. Other peaks are of the Tl, Ba, Ca, Cu, or O character spectrum. All these results are consistent with the X-ray diffraction experiments.

### III. OPTICAL PROPERTIES

Optical spectroscopy measurement can yield rich information about charge dynamics of a system. Intensive optical studies have been done on La-, Y-, and Bi-based cuprate systems, comparatively, much less optical investigations have been done on Tl-based systems. As we mentioned in the introduction, infrared studies on the Tl-based systems have been performed only on single-layer and double-layer compounds near optimal doping. Therefore, in this work, we shall mainly focus on the data of Tl-2223 crystals, as well as their comparisons with data of Tl-2201 and Tl-2212.

The reflectance measurements from 100 to 22000  $\text{cm}^{-1}$  were carried out on a Bruker 66v/S spectrometer. An in-situ overcoating technique was used for the experiment[19]. The optical conductivity spectra were derived from the Kramers-Kronig transformation. Hagen-Rubens relation was assumed for the low-

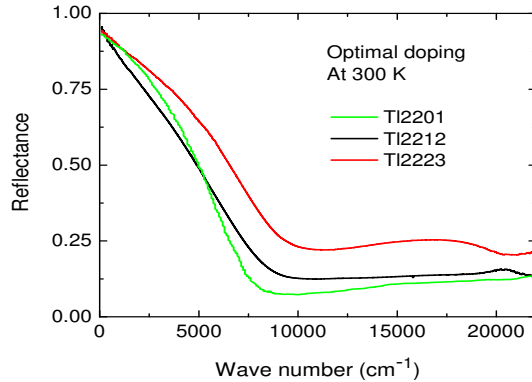


FIG. 6: The reflectance data of Tl-2201, Tl-2212 and Tl-2223 crystals up to  $22000\text{ cm}^{-1}$  at room temperature.

frequency extrapolation. At high frequency side, a constant extrapolation was adopted up to  $1,000,000\text{ cm}^{-1}$ , then a  $R(\omega) \sim \omega^{-4}$  was used. A comparison of the in-plane reflectances of Tl-2201, Tl-2212 and Tl-2223 single crystal at room temperature is shown in Fig. 6. Clearly as the  $\text{CuO}_2$  layers of a unit cell goes from 1 to 3, the plasma edge goes to higher energy. The observation indicates that the carrier density increases with increasing the number of  $\text{CuO}_2$  layers in a unit cell.

Fig.7 (a) and (b) show the reflectance  $R(\omega)$  and conductivity  $\sigma_1(\omega)$  spectra for a Tl-2223 crystal at different temperatures. In the high temperature, the Tl-2223 reflectance spectra show roughly linear frequency dependence, a behavior common to all hole-doped high- $T_c$  cuprates. The linear frequency dependence of  $R(\omega)$  implies a linear variation of the inverse lifetime of carriers with frequency, which could be well described by a marginal Fermi liquid theory.[20] With decreasing temperature, the low- $\omega$   $R(\omega)$  increases, indicating a metallic response of the sample. At 10 K in the superconducting state,  $R(\omega)$  shows a clear knee structure at around  $600\text{ cm}^{-1}$ . Above this frequency, the reflectance drops fast and becomes lower than the normal-state values at around  $1000\text{ cm}^{-1}$ .  $R(\omega)$  recovers the linear-frequency dependence at higher frequency about  $1600\text{ cm}^{-1}$ . Similar but slightly weak behaviors were seen at 90 K, which is close to  $T_c$ . The change of  $R(\omega)$  in the superconducting state with respect to the normal state could be seen more clearly from the plot of the ratio of the reflectance below  $T_c$  over that above  $T_c$ .

Fig.8 shows the ratio of  $R_{10K}(\omega)/R_{130K}(\omega)$  as a function of frequency. Also, the  $R_{10K}(\omega)/R_{120K}(\omega)$  of a Tl-2212 crystal is included for comparison. Obviously both of them have a maximum and a minimum in the plot. The values near the maximum have much noise, however, we can see clearly the dip minimum and the fitting maximum of Tl-2223 shift to higher energy compared with Tl-2212[18].

A useful way to display in-plane infrared data is in terms of the optical life time of the carriers which can be extracted from the conductivity data using the extended

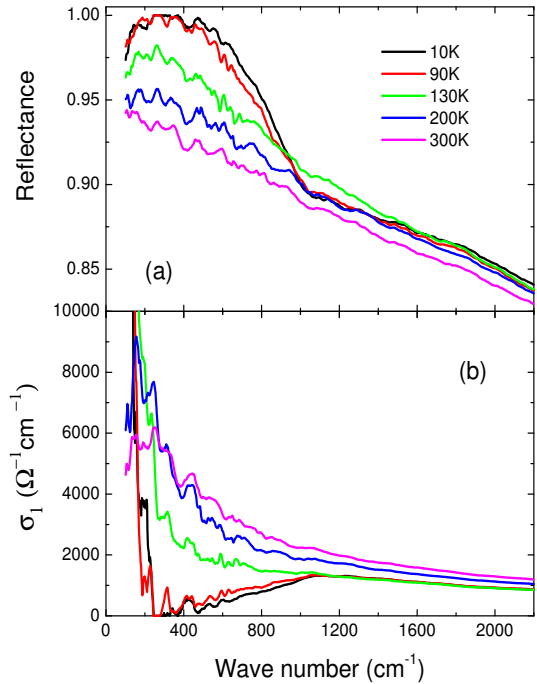


FIG. 7: ab-plane optical data of the optimally doped Tl-2223 single crystal with  $T_c=119\text{ K}$ . (a) The temperature dependent reflectance and (b) the temperature-dependent  $\sigma_1(\omega)$ .

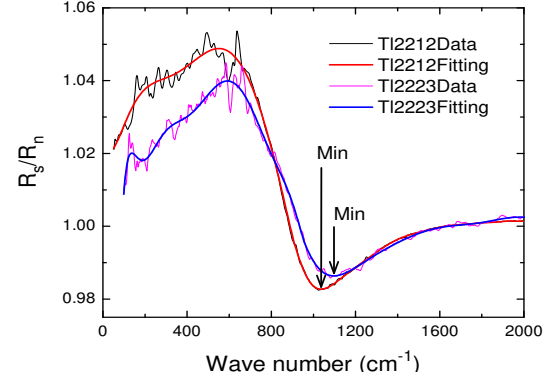


FIG. 8: The  $R_s(\omega)/R_n(\omega)$  from  $100$  to  $2200\text{ cm}^{-1}$  of the optimally doped Tl-2223 single crystal with  $T_c=119\text{ K}$ . The Tl-2212 data is included for comparison.

Drude formalism. The reciprocal of the lifetime, or the scattering rate,  $1/\tau(\omega)$ , is defined as[17]

$$\tau^{-1}(\omega) = \frac{\omega_p^2}{4\pi} \frac{\sigma_1(\omega)}{\sigma_1^2(\omega) + \sigma_2^2(\omega)}, \quad (1)$$

where  $\omega_p$  is the plasma frequency. The scattering rate  $1/\tau(\omega)$  for 10 K and 130 K and 300 K data are shown in Fig.9, extracted from Eq.(1) using the plasma frequency  $20,000\text{ cm}^{-1}$ , determined by summarizing the optical conductivity up to the plasma edge near  $8,000\text{ cm}^{-1}$ . The  $1/\tau(\omega)$  at 300 K is linear in the low energy range. However,  $1/\tau(\omega)$  at 10 K exhibits a rapid rise and

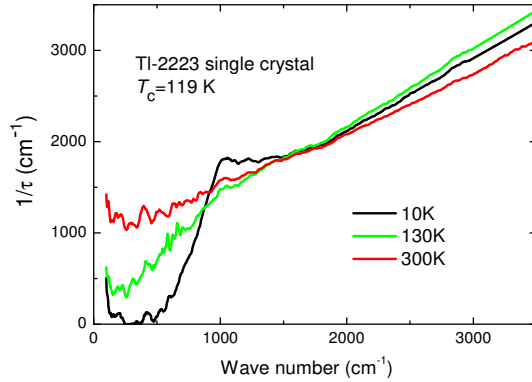


FIG. 9: Optical scattering rate spectra from 100 to 3500  $cm^{-1}$  of the optimally doped Tl-2223 single crystal with  $T_c=119K$ .

a substantial overshoot of the normal-state spectrum at the frequencies corresponding to the maximum and minimum in the  $R_{10K}(\omega)/R_{130K}(\omega)$  plot (in Fig.8), respectively. Above this range the scattering rate in the superconducting state becomes linear up to several thousand wave number.

The sharp rise and the overshoot in  $1/\tau(\omega)$  at low T are quite similar to other high- $T_c$  cuprates. The difference is that the energy scales of the characteristic features for Tl-2223 are higher than that for Tl-2212 compound. In our earlier study[18], we already showed that the same structures in  $1/\tau(\omega)$  on Tl-2212 system with  $T_c=108$  K are substantially higher than systems with  $T_c$  around 90 K. A comparison of the scattering rate for the three phases at 10 K is shown in Fig.10. In this plot, the data for Tl-2201 crystal near optimal doping are taken from Puchkov's work[16]. The energy shifts of both the sharp rise and the overshoot structures are seen rather clearly. In fact, the energy scales of those features continue to shift up in compounds with higher superconducting transition temperature. This can be seen very clearly from optical work done on Hg-1223 with  $T_c\sim 130$  K[21].

The characteristic features were widely believed to result from the interaction of electrons with a collective mode in combination with a superconducting gap that appears below  $T_c$ [22, 23, 24, 25, 26]. In photoemission experiment, a kink in the dispersion along the zone diagonal develops in the low temperature which is due to the correction by the real part of self-energy of quasiparticle, and by Kramers-Kronig relation, a rapid broadening of the photoemission line width, i.e. a sudden change of the life time of quasiparticle is seen simultaneously[1]. The enhanced absorption above the knee frequency in infrared response results from an enhanced scattering, which should have the same origin as the line width broadening or the kink in the dispersion observed along the zone diagonal in ARPES. Extracting the Bosonic spectral function from the infrared spectra has been established theoretically by performing second derivative of the optical scattering rate multiplied by frequency

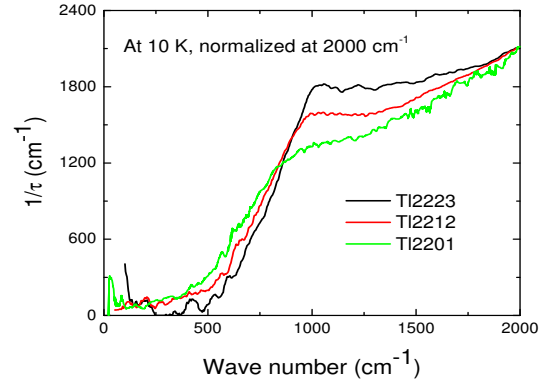


FIG. 10: Optical scattering rate spectra from 200 to 2000  $cm^{-1}$  of the optimally doped Tl-2201, Tl-2212 and Tl-2223 single crystals. Data for Tl-2201 with  $T_c=88$  K (very close to the optimal doping) are taken from ref.[16]. The data have been normalized to Tl-2223 at 2000  $cm^{-1}$ .

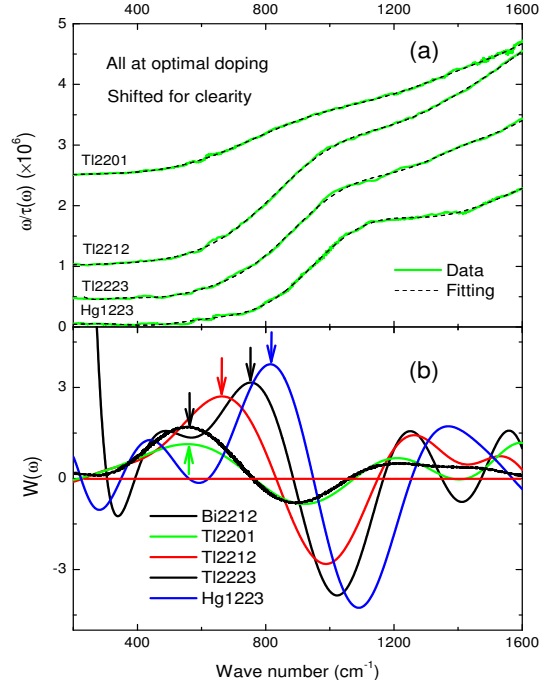


FIG. 11: (a) Scattering rate data multiplied by  $\omega$  for Tl-2201, Tl-2212, Tl-2223, and Hg-1223. The scattering data for Tl-2201 were taken from [16], the data for Hg-1223 from [21]. The curves are shifted vertically for clarity. (b) The spectral function  $W(\omega)$  at 10 K (in the superconducting state) derived from the polynomial fitting. The data for Bi-2212 were taken from [25]. The arrows indicate the positions of main peaks.

through[22, 27]:

$$W(\omega) = \frac{1}{2\pi} \frac{d^2}{d\omega^2} [\omega \frac{1}{\tau(\omega)}], \quad (2)$$

As such second derivative contains detectable singularities at a number of characteristic energies, the inversion method was widely used to determine the parameters like

gap amplitude  $\Delta$  and Boson mode energy  $\Omega$ .

Fig. 11(a) shows the plot of the scattering rate multiplied by frequency vs. frequency for Tl-2201, Tl-2212, and Tl-2223 crystals. The data for Hg-1223 crystal taken from ref.[21] are also plotted. Then, the curves were fitted with a high-order (40 orders) polynomial. To see the energy scales of the features more clearly, we have shifted the curves vertically for different compounds. The spectral functions  $W(\omega)$  obtained by equation (2) are plotted in Fig. 11(b). The  $W(\omega)$  data for a high-quality Bi-2212 crystal with  $T_c=91$  K obtained by Tu et al. are also added[25]. We can see clearly that, for those systems with different  $T_c$  at optimal doping, the positive maximum and the negative minimum increase systematically with  $T_c$ .

Although it is generally agreed that the second derivative of the optical conductivity, i.e. the  $W(\omega)$  spectrum, reflects the bosonic spectral function, different opinions exist regarding to the energy positions of the positive maximum and the negative minimum. Considering a d-wave gap symmetry, Carbotte et al.[22, 23] argued that the peak in  $W(\omega)$  below  $T_c$  occurs at  $\Delta+\Omega$ , while the minimum is at  $2\Delta+\Omega$ . However, Abanov et al.[24] argued that the d-wave gap does not affect the threshold position in conductivity, as a result, a sharp maximum in  $W(\omega)$  occurs at  $2\Delta+\Omega$  followed by a deep minimum. They emphasized that at  $T=0$  K the maximum and minimum are at the same frequency, while at finite temperature, the maximum shifts to low frequency, but the minimum remains at the same frequency as at  $T=0$  K. So, they also identify the  $2\Delta+\Omega$  with the deep minimum in  $W(\omega)$ . If we accept that the peak in  $W(\omega)$  locates at  $\Delta+\Omega$ , and the minimum is at  $2\Delta+\Omega$ , we obtained a plot for the peak and the dip energy as a function of  $T_c$  for the different systems at optimal doping, as shown in Fig. 12. Obviously, both of them scale well with  $T_c$  for different systems. Furthermore, the difference between them should give the superconducting gap energy  $\Delta$ . In the figure, we also make the plot for the energy difference between the dip and the peak vs  $T_c$ . It then shows a trend of increase with decreasing the superconducting transition temperature  $T_c$  for different systems. This is not physically reasonable, and also in contradiction to the ARPES experimental results which show a decrease of the gap for the systems with lower  $T_c$ [28, 29]. We think that the current analysis puts new challenge to the established models.

Nevertheless, the linear scaling of the energy of the peak (and also the dip) in  $W(\omega)$  with  $T_c$  is firmly established in our experiment. At present, the nature of the mode is not clear. It is still under dispute whether the mode is a phonon or a magnetic resonance as detected by neutron scattering experiment. If the maximum or minimum indeed involve a sum of the gap  $\Delta$  and a Boson mode  $\Omega$ , then the scaling behavior not only means that the gap amplitude  $\Delta$  is proportional to  $T_c$ , but Boson mode energy  $\Omega$  is also proportional to  $T_c$  for the different systems. In this case, the phonon origin for the Boson

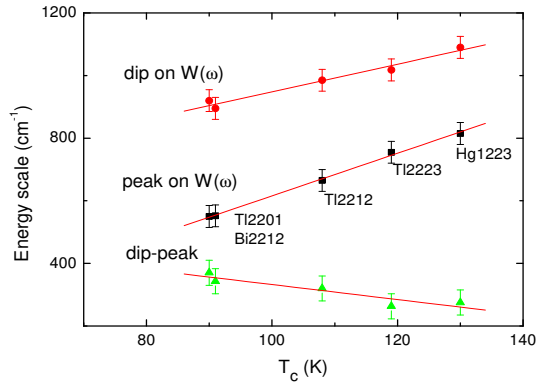


FIG. 12: The energy scales of the negative dip and the main peak vs.  $T_c$  for several optimally doped cuprates. The energy difference between the dip and the peak is extracted simply.

mode is unambiguously ruled out, because the in-plane phonon is determined by the Cu-O bond length, which should not change with systems for different  $T_c$ .

However, we would also like to point out that the above scenario of a mode plus a gap for the reflectance feature below  $T_c$  relies on the clean limit of the ab-plane superconductivity. The unreasonable result obtained from the energy difference between the dip and the peak in terms of the model by Carbotte et al.[22] may suggest that the ab-plane of high- $T_c$  cuprates is not in clean limit. In the case of dirty limit, on the other hand, the sharp rise feature in the scattering rate should be at  $2\Delta$ , since the impurities elastic scattering should be able to transfer the momentum of the particle-hole excitations without affecting the threshold energy. At present, there is still no agreement on whether or not the ab-plane is in clean limit. Very recently, Homes[30] suggests that the criteria of a small value of the quasiparticle scattering rate for  $T \ll T_c$  is not a good measure of whether or not the superconductivity is in the clean or dirty limit. By contrast, The normal-state value of  $1/\tau$  should be considered when determining whether a system is in the clean or dirty limit. They also pointed out that the clean-limit requirement is much more stringent for a d-wave system than it is for a material with an isotropic energy gap, since it not only requires  $1/\tau$  much less than the maximum gap amplitude, but also  $1/\tau \leq 2\Delta_k$  in the nodal regions. They established a linear scaling relation  $\rho_s \propto \sigma_{dc} T_c$  for cuprates, and argued that this scaling is the hallmark of a dirty-limit system. In a dirty-limit case, no Boson mode would be involved in the sharp rise of scattering rate, or the main peak in the spectral function  $W(\omega)$ . The feature would be purely due to the singularity of density of state at gap position. Then what we observed and analyzed in this work only reflect the variation of the gap amplitude in systems with different  $T_c$ . At present, it need rather sufficient experimental data and more theoretical efforts to identify whether the ab-plane superconductivity in cuprates is in the dirty-limit.

#### IV. SUMMARY

In conclusion, single crystal Tl-2223 were grown by flux method. All crystals were of the platelet form, from 1 to  $2\text{mm}^2$ . They were characterized by ac susceptibility, X-ray diffraction, SEM and EDX analysis. The optical properties were investigated for the crystals with focus on the Tl-2223 compounds. The reflectance spectrum exhibits a knee structure at around  $600\text{ cm}^{-1}$  and a dip at higher frequency below  $T_c$ . The ratio of the reflectance below and above  $T_c$  displays a maximum and pronounced minimum at the knee and dip frequencies. The scattering rate and its second derivative were extracted and compared with other cuprate systems. A linear scaling be-

havior for the maximum and the negative minimum with  $T_c$  is established for systems with different  $T_c$  at optimal doping. We discussed the physical consequences of the experimental data in terms of both clean and dirty limits. At present, it is an open question whether the ab-plane of HTSCs are in the clean or dirty limit.

#### Acknowledgments

We wish to acknowledge senior engineer H.Chen for her help in XRD experiment. This work is supported by the National Natural Science Foundation of China.

---

[1] M. R. Norman and C. C. Pépin, *Rep. Prog. Phys.* **66** (2003) 1547.  
[2] H. A. Mook, M. Yethraj, G. Aeppli, T. E. Mason and T. Armstrong, *Phys. Rev. Lett.* **70** (1993) 3490.  
[3] H. Ding, T. Yokoya, J. C. Campuzano, T. Takahashi, M. Randeria, M. R. Norman, T. Mochiku, K. Kadowaki and J. Giapintzakis, *Nature* **382** (1996) 51.  
[4] A. G. Loeser, Z. X. Shen, D. S. Dessau, D. S. Marshall, C. H. Park, P. Fournier and A. Kapitulnik, *Science* **273** (1996) 325.  
[5] S. W. Cheong, G. Aeppli, T. E. Mason, H. Mook, S. M. Hayden, P. C. Canfield, Z. Fisk, K. N. Clausen, and J. M. Martinez, *Phys. Rev. Lett.* **67** (1991) 1791.  
[6] H. He, P. Bourges, Y. Sidis, C. Ulrich, L. P. Regnault, S. Pailhes, N. S. Berzigerova, N. N. Kolesnikov and B. Keimer, *Science* **295** (2002) 1045.  
[7] H. F. Fong, P. Bourges, Y. Sidis, L. P. Regnault, A. Ivanov, G. D. Gu, N. Koshizuka and B. Keimer, *Nature* **398** (1999) 588.  
[8] S. S. P. Parkin, V. Y. Lee, A. I. Nazzal, R. Savoy, T. C. Huang, G. Gorman and R. Beyers, *Phys. Rev. B* **38** (1988) 6531.  
[9] H. Ihara, R. Sugise, K. Hatashi, M. Terada, M. Jo, N. Hirabayashi, A. Negishi, N. Atoda, H. Oyanagi, T. Shimomura and S. Ohashi, *Phys. Rev. B* **38** (1988) 11952.  
[10] Z. Sheng and A. M. Hermann, *Nature* **332** (1988) 138.  
[11] Toshihiro KOTANI, Tetsuyuki KANEKO, Hiromi TAKEI and Koji TADA, *Jap. J. appl. Phys.* **28** (1989) 1378.  
[12] A. Maignan, C. Martin, V. Hardy, Ch. Simon, M. Hervieu and B. Raveau, *Physica C* **219** (1994) 407.  
[13] S. Kondoh, Y. Ando, M. Onoda and M. Sato, *solid state commun.* **65** (1988) 1329.  
[14] S. S. P. Parkin, V. Y. Lee, E. M. Engler, A. I. Nazzal, T. C. Huang, G. Gorman, R. Savoy, and R. Beyers, *Phys. Rev. Lett.* **60** (1988) 2539.  
[15] N. Merrien, L. Coudrier, C. Martin, A. Maignan, F. Studer, and A. M. Flank, *Phys. Rev. B* **49** (1994) 9906.  
[16] A. V. Puchkov, T. Timusk, S. Doyle, and A. M. Hermann, *Phys. Rev. B* **51** (1995) 3312.  
[17] A. V. Puchkov, D. N. Basov and T. Timusk, *J. Phys. C* **8**, 10049 (1996).  
[18] N. L. Wang, P. Zheng, J. L. Luo, Z. J. Chen, S. L. Yan, L. Fang, Y. C. Ma, *Phys. Rev. B* **68**, 054516 (2003).  
[19] C. C. Homes, M. Reedyk, D. A. Crandles, and T. Timusk, *Appl. Opt.* **32**, 2976 (1993).  
[20] J. Hwang, T. Timusk, A. V. Puchkov, N. L. Wang, G. D. Gu, C. C. Homes, J. J. Tu, and H. Eisaki, *Phys. Rev. B* **69**, 094520 (2004).  
[21] J. J. McGuire, M. Windt, T. Startseva, T. Timusk, D. Colson and V. Viallet-Guillen, *Phys. Rev. B* **62**, 8711 (2000).  
[22] J. P. Carbotte, E. Schachinger, and D. N. Bosov, *Nature* **401**, 354 (1999).  
[23] E. Schachinger and J. P. Carbotte, *Phys. Rev. B* **64**, 094501 (2001).  
[24] A. Abanov, A. V. Chubukov, and J. Schmalian, *Phys. Rev. B* **63**, 180510(R) (2001).  
[25] J. J. Tu, C. C. Homes, G. D. Gu, D. N. Basov, and M. Strongin, *Phys. Rev. B* **66**, 144514 (2002).  
[26] J. Hwang, T. Timusk, and G. D. Gu, *Nature* **427**, 714 (2004).  
[27] F. Marsiglio, T. Startseva, and J. P. Carbotte, *Phys. Lett. A* **245**, 172 (1998).  
[28] H. Matsui, T. Sato, T. Takahashi, H. Ding, H.-B. Yang, S.-C. Wang, T. Fujii, T. Watanabe, A. Matsuda, T. Terashima, and K. Kadowaki, *Phys. Rev. B* **67**, 060501(R) (2003).  
[29] D. L. Feng, A. Damascelli, K. M. Shen, N. Motoyama, D. H. Lu, H. Eisaki, K. Shimizu, J.-i. Shimoyama, K. Kishio, N. Kaneko, M. Greven, G. D. Gu, X. J. Zhou, C. Kim, F. Ronning, N. P. Armitage, and Z.-X Shen, *Phys. Rev. Lett.* **88**, 107001 (2002).  
[30] C. C. Homes, S. V. Dordevic, T. Valla, and M. Strongin arXiv: cond-mat/0410719.